Noncontact Electrical System Monitoring on a U.S. Coast Guard Cutter

Peter Lindahl, Greg Bredariol, John Donnal, and Steven Leeb

Modernization in the U.S. Navy and U.S. Coast Guard (USCG) includes an emphasis on automation systems to help replace manual tasks and reduce crew sizes. This places a high reliance on monitoring systems to ensure proper operation of equipment and to maintain safety at sea. Recently developed noncontact current and voltage sensors, [1] combined with nonintrusive load monitoring (NILM) methods [2], provide a nonintrusive, low-cost, and easily installed package for machinery monitoring. This paper presents an application case study using these NILM-enabled sensors installed on the main electrical feeders of the USCG Famous Class Cutter SPENCER. The system records the power demand on the ship and disaggregates this demand by identifying transients corresponding to loads changing states, e.g., a pump turning on. Results of this study showcase these novel sensors' ability to monitor both generation and load-side equipment while at sea or in port and provide information useful for tracking operation schedules, energy usage, and maintenance needs.

NILM on the USCGC SPENCER

The USCG Cutter (USCGC) SPENCER (Fig. 1) is a 270 ft. (82 m) Medium Endurance vessel stationed in Boston, MA. Commissioned in 1986, the SPENCER hosts a 100-person crew and conducts operations providing environmental stewardship, law enforcement, fisheries protection, and national security. The ship has an operational tempo of 185 days at sea each year, with each patrol typically requiring 1 to 2 months away from homeport.

The ship's primary electrical generation plant consists of two 475 kW V12 Caterpillar diesel generator sets, which provide the ship's electrical power when at sea. When in a port with sufficient electrical service, the ship can receive power from shore via one of two feeder systems. Each shore tie consists of four TSGU-200 cables (each cable contains one 4/0 stranded copper conductor per phase), while each feeder connecting the onboard generators to the main switchboard consists of three TSGU-200 cables. The USCGC SPENCER's electrical distribution system is a delta-configured 254/440 V system, and electric loads on the vessel range from large (tens of kW) three-phase loads (such as salt water cooling pumps, HVAC equipment, fire protection pumps, and hydraulic systems) to smaller (hundreds of W) line-line loads including lights, washers and driers, and ovens.

Recently developed noncontact power meters [1] provide an opportunity to monitor the ship's microgrid without an intrusive retrofit. These meters do not require an ohmic contact for voltage measurements and can be installed on the outside of the multiphase cables of the generator and shore tie feeders. Thus, they are quick and safe to install, and doing so does not require interrupting electrical service or compromising waterproof equipment. Further, incorporating NILM capabilities, i.e., the ability to disaggregate this centrally recorded

Fig. 1. The US Coast Guard Cutter SPENCER at sea [3].

This paper was presented at IEEE AUTOTESTCON 2016 (© IEEE 2016, used with permission, [13].)
It has been slightly edited and formatted for the *IEEE I&M Magazine*.
Acknowledgment: The authors thank the Office of Naval Research NEPTUNE Program and the Grainger Foundation for their financial and technical support.

1094-6969/17/$25.00©2017IEEE

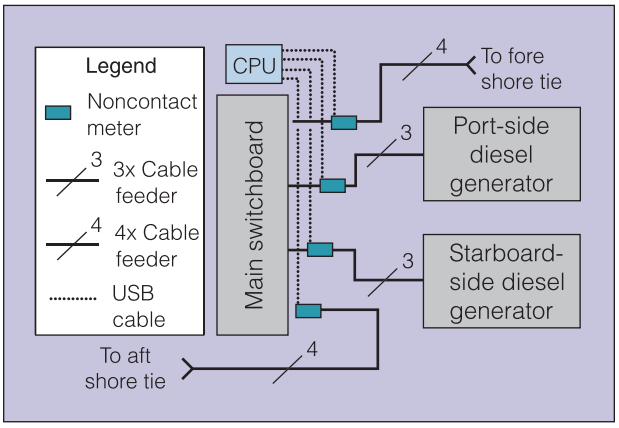

Fig. 2. Diagram of the USCGC SPENCER's electrical supply to the main switchboard. Noncontact sensors installed on each feeder collect current and voltage data and transmit this data to a nearby central computer via USB cables.

power data into individual load information through transient identification [2], [4], allows individual machinery monitoring without a widespread sensor network. The potential advantages of the NILM approach are lower equipment and installation costs and increased reliability.

Fig. 2 diagrams the ship's electrical supply to the main switchboard and the installation of the noncontact meters. As shown, the meters' outputs are transmitted via USB to a central computer. This computer is outfitted with a custom NILM database (NILMdB) [5] and operating software (NILM Manager) [6] designed for efficient data storage, retrieval, and load identification.

The Noncontact NILM Package

Fig. 3 shows an installation of a noncontact sensor package around a multi-conductor cable. The sensor package consists of a main sensor board containing a single Hall effect sensor circuit and a single capacitive pick-up sensor circuit, plus a microcontroller for data acquisition and transmission

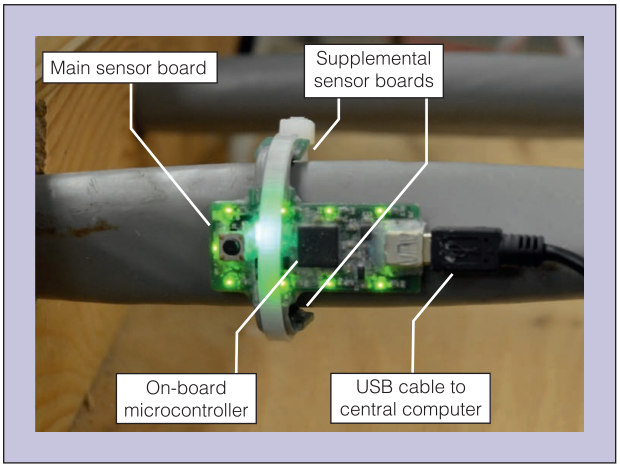

Fig. 3. The noncontact sensors installed on the outside of a multiphase cable.

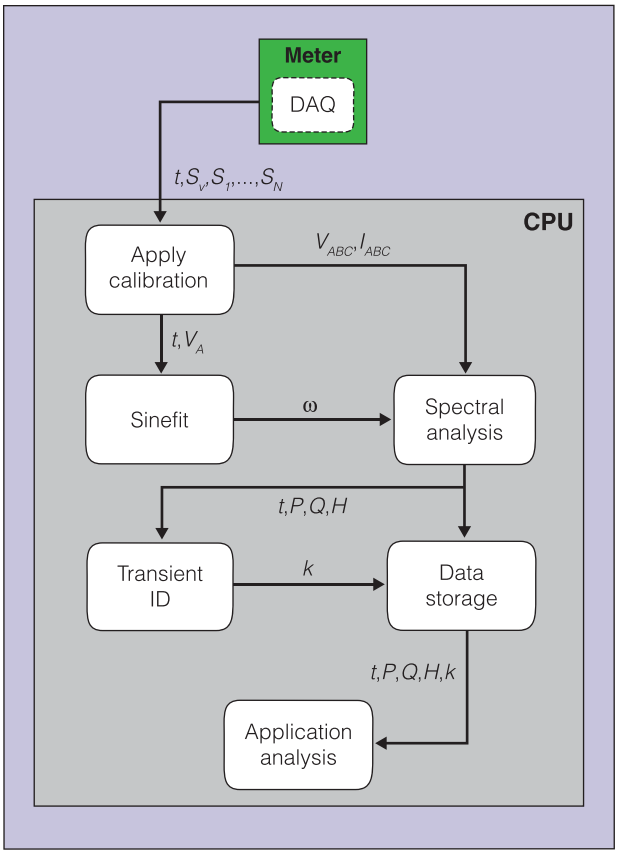

Fig. 4. Data flow and processing pipeline for converting raw sensor measurements into real, reactive, and harmonic power data useful for application analysis.

to the central computer. Supplemental Hall effect sensor boards attach to the main board via ribbon cables. The Hall effect sensors collect point-measurements of the magnetic field surrounding the cable, while the capacitive pick-up sensor measures the electric field. When combined with a calibration process, the Hall effect sensors provide measurements of the per-phase currents inside the cable, and the capacitive pick-up sensor provides the information for determining the instantaneous line-frequency and phase relationships of these currents and their corresponding phase voltages. The central computer processes these measurements into power streams containing real, reactive, and harmonic components. These power streams are then scanned for transients that match known exemplars corresponding to specific loads turning on or off. This data and processing flow is depicted in Fig. 4.

Current Sensors

Fig. 5 shows a schematic for each current sensor. The sensor consists of an Allegro MicroSystem's A1362 Hall Effect sensor chip buffered (the AD8676 op-amp) and capacitively coupled to a double-gain stage amplifier (two AD8513 op-amps). The chip has a programmable gain of up to 16 mV/G, sufficient for standard electrical system current levels. The 2.2 μF capacitor and 49.9 kΩ input resistance to the gain stages acts to high-pass

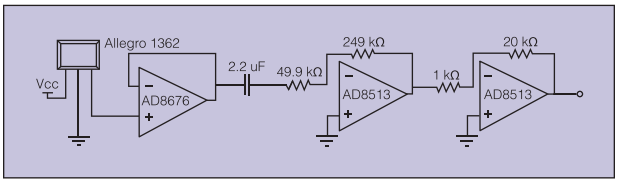

Fig. 5. Schematic for the Hall effect current sensor.

the measured signal at 1.5 Hz. This serves to reduce effects of low-frequency drift and avoid signal saturation.

Voltage Sensors

To determine phase voltage information, a differential capacitive-pickup sensor measures the electric field emanating from a conductor or multi-conductor cable. This sensor has the schematic shown in Fig. 6. The differential inputs to the AD8421 instrumentation amplifier are connected to copper plates on the main PCB. Each plate creates a capacitive coupling with the conductor of interest. Along with the 1 MΩ resistors, these capacitances create an input stage transfer function with the form:

$$H(s) = \frac{sRC}{sRC+1} \tag{1}$$

While the 1 MΩ bias resistors are large, the mutual capacitance between the conductor and sensor is very small, on the order of picofarads. As such, RC is small, and (1) reduces the transfer function of a differentiator, i.e., $H(s) \approx sRC$ at the line of frequency (60 Hz) and its first several harmonics. Thus, the instrumentation amplifier is followed by an integrator to recover the voltage. An inverting op-amp provides signal gain. In addition, an integrator circuit provides feedback to the reference pin of the instrumentation amplifier, which eliminates offsets and low-frequency drift in the signal.

Data Sampling and Communication with Central Computer

The outputs of each sensor are sampled at a rate of 3 kHz by the built in 12-bit ADC of the Atmel SAM4S microcontroller on the main board of the noncontact meter package. This sample rate and bit-resolution are sufficient for capturing the fundamental amplitude and phase relationships of the current and voltage measurements as well as several harmonic components. Following sampling, the microcontroller transmits the sensor outputs via USB to the central computer for subsequent processing into power streams.

Nonintrusive Calibration of Sensors

The drawback to using "point" reference sensors is that the magnetic and electric fields vary by position around the conductor of interest and decrease in strength with distance. Further, if other conductors are nearby (as is necessarily the case in multi-conductor cables), the magnetic and electric fields in the space around the cable are linear combination of fields due to each conductor's current and voltage, respectively. Thus, it is necessary to calibrate the sensors for disaggregating individual phase power streams.

Phase Currents and Current Sensors Relationship: Assuming no ground faults in the ship's Delta-configured microgrid, the phase current relationship for each feeder is:

$$I_A + I_B + I_C = 0 \tag{2}$$

This means that the currents only span two dimensions as one current is always a linear combination of the other two. Then, the output of an N-length Hall effect sensor network monitoring the conductors depend on only two phases, i.e.:

$$\begin{bmatrix} S_1 \\ S_2 \\ \vdots \\ S_N \end{bmatrix} = \begin{bmatrix} m_{1A} & m_{1B} \\ m_{2A} & m_{2B} \\ \vdots & \vdots \\ m_{NA} & m_{NB} \end{bmatrix} \begin{bmatrix} I_A \\ I_B \end{bmatrix} \tag{3}$$

Here, each m term corresponds to the sensor output contribution of the two independent phase currents. As long as the sensor network spans the current space, i.e., the sensors are located around the conductors such that they sufficiently measure the independent currents, then knowing these m terms allows the calculation of currents from sensor measurements via (2) and:

$$\begin{bmatrix} I_A \\ I_B \end{bmatrix} = \mathbf{K} \begin{bmatrix} S_1 \\ S_2 \\ \vdots \\ S_N \end{bmatrix} \tag{4}$$

Here, $\mathbf{K}$ is the pseudoinverse of the m terms matrix in (3). For each meter installation aboard the ship, four Hall effect sensors were used so $N = 4$ in (3) and (4).

Phase Voltages and the Voltage Sensor Relationship: For a three-phase electrical distribution system, the phase voltages are related as:

$$V_A(t) = V\cos(\omega t) \tag{5}$$

$$V_B(t) = V\cos\left(\omega t - \frac{2\pi}{3}\right) \tag{6}$$

$$V_C(t) = V\cos\left(\omega t + \frac{2\pi}{3}\right) \tag{7}$$

Thus, the electric field sensor output is a linear combination of voltages with the same frequency, and itself will be a single sinusoid of the form:

$$S_V(t) = A\cos(\omega t + \phi) \tag{8}$$

where ϕ represents the phase-relationship between the measured sensor output and V_A.

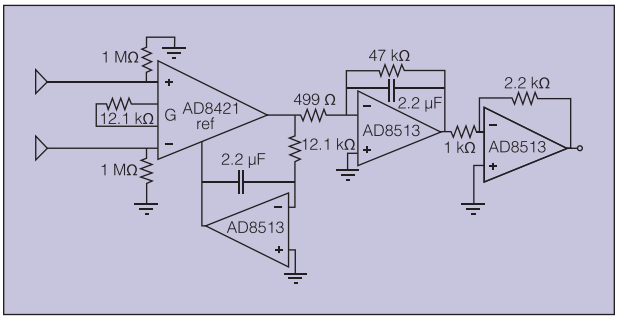

Fig. 6. Schematic for capacitive pick-up voltage sensor.

Nonintrusive Calibration Procedure: To calibrate the noncontact sensors without interrupting service, a resistive load is pulse-width modulated (PWM) to create a discernible signal in the measured currents amongst the intrinsic shiploads, which are treated as background noise. In this way, the calibration load can be differentiated from the background loads using spectrum analysis. This method leverages the superposition principle to calibrate the sensors. It should be noted that the accuracy of this method depends on the linear response of the sensors; therefore, this method fails if the Hall effect sensors saturate or if circuitry gains cause signals to clip.

Using a microcontroller and a solid-state relay (SSR), the calibration load, an 8.5 kW heater is cycled at a frequency of 0.33 Hz and duty cycle of 33%. This oscillating load is connected across phases $A - C$ for 90 seconds and then $B - C$ for 90 seconds. During this process, the NILM software on the central computer takes the fast Fourier transform (FFT) of the current sensor measurements and finds the fundamental and harmonic components corresponding to the PWM calibration load. These components are then matched against the Fourier series coefficients of a PWM signal. This process allows the computer to determine the $m_{1A} - m_{4A}$ terms of (3) when the load is across phases $A - C$ (at this time $I_B = 0$), and the $m_{1B} - m_{4B}$ terms when the load is across phases $B - C$ ($I_A = 0$). With these terms known, the matrix $\mathbf{K}$ is known, and the current sensors are calibrated.

Assuming (5) – (7) hold, i.e., the ship's voltages are stiff with constant phase relationships, only A and ϕ are required to convert the measured signal of (8) to the voltages of (5) – (7). When the load is connected from V_A to V_C, the load current has the form:

$$I_L(t) = \sqrt{3}\frac{V}{R}\cos\left(\omega t - \frac{\pi}{6}\right) \tag{9}$$

where R is the resistive value of the load. With I_L available from the calibrated current sensors, ϕ can be calculated as:

$$\phi = \theta - \frac{\pi}{6} \tag{10}$$

where θ is the phase difference between S_V (8) and I_L (9). Collectively then, V_A, V_B, and V_C can then be estimated by scaling S_V by the factor $\frac{V}{A}$ and phase shifting the waveforms in accordance with (5) – (10).

Power Calculations

Once calibration is achieved, the Sinefit algorithm and spectral envelope processor [7] runs on the central computer to produce phase power and harmonic calculations. This processor effectively fits a sinusoid to one voltage stream over a single line-cycle to estimate the instantaneous frequency and provides that frequency for the spectral analysis of the current measurements. The outcome is the compression of information into three-phase real (P) and reactive power components (Q) as well as 3rd, 5th, and 7th current harmonics (H) at a rate equivalent to the line-frequency (60 Hz in the case of the ship's main distribution system).

In laboratory settings, power estimates achieved using noncontact current and voltage sensors have shown accuracies to within 1% of the power reported by a conventional power meter. The accuracy of these meters, however, is highly affected by the installation and calibration process. Most notably, the Hall effect sensors can show nonlinear effects including saturation and hysteresis [1] if the magnetic field emanating from the wire is too strong. This can happen if the sensor is installed too close to the conductor (for example, if the conductor insulation and cable jacket are thin). In this case, the sensor requires "spacers" between itself and the cable. The time-length of the calibration process also affects power measurement accuracy, as do the characteristics of the concurrent loads on the electrical system.

Transient Identification

For identifying individual load transients in these power streams, a correlation-based event identification algorithm, Trainola [5], is built into the NILM system. In this algorithm, a measure of the correlation between an exemplar, i.e., a recorded or modeled transient event of a specific load, and an equivalent-length section of electrical data is calculated as the window moves across a data stream. When this measure peaks within a defined range, the algorithm marks the time instance corresponding to the beginning of the moving window as that of an event corresponding to the exemplar.

Consider an exemplar, g, of length T, and the equal-length windowed portion of a data stream, f. The sum of squared errors between these two waveforms is defined as:

$$E = \sum_{n=1}^{T}\left(f[n] - g[n]\right)^2 \tag{11}$$

This error term can be expanded and ultimately rewritten in terms of dot products, i.e.:

$$E = \sum_{n=1}^{T} f^2[n] + \sum_{n=1}^{T} g^2[n] - 2\sum_{n=1}^{T} f[n]g[n] \tag{12}$$

$$E = (f\cdot f) + (g\cdot g) - 2(f\cdot g) \tag{13}$$

$$E = |f|^2 + |g|^2 - 2(f\cdot g) \tag{14}$$

If the waveforms are identical, the sum of squared errors term

is $E = 0$, and (14) can be reformed as:

$$f \cdot g = \frac{|f|^2 + |g|^2}{2} \tag{15}$$

Further, if the magnitudes of the exemplar and the measured waveform are the same, i.e. $|g| = |f|$, then (15) reduces to:

$$\frac{f \cdot g}{|f|^2} = 1 \tag{16}$$

Thus, we can define a function for each power stream and each exemplar:

$$M[k] = \frac{f \cdot g}{|g|^2} \tag{17}$$

that generates a local maximum with a value around 1 when the windowed section, f, of a data stream starting at time instance, k, matches well in amplitude and shape to exemplar, g. When Trainola detects this peak, it creates a marker indicating the time of the corresponding event.

Fig. 7 helps to understand the performance of the Trainola algorithm. The top two plots show the real and reactive power streams that contain a fire pump turn-on event at approximately the 14-second mark. The pump later turns off around the 28-second mark. All other transients in the streams are other loads. To find this turn-on event, as the computer receives this data, the Trainola algorithm effectively sweeps the 3-second fire pump turn-on exemplars across the streams. When the exemplar time-aligns with the transient, the algorithm metric for the real and reactive power stream, M_P and M_Q, respectively, results in positive peaks values of 0.87 and 0.94, respectively. Both are very close to the ideal value of 1. This process can be repeated for each phase and harmonic for a multidimensional analysis. It should be noted that the Trainola identification method is not robust to time-domain changes in transients, such as a significant increase in peak power or an increase in the time the transient takes to decay to steady state. Ultimately, transient exemplars might need periodic updating if using this method for disaggregation over long time periods.

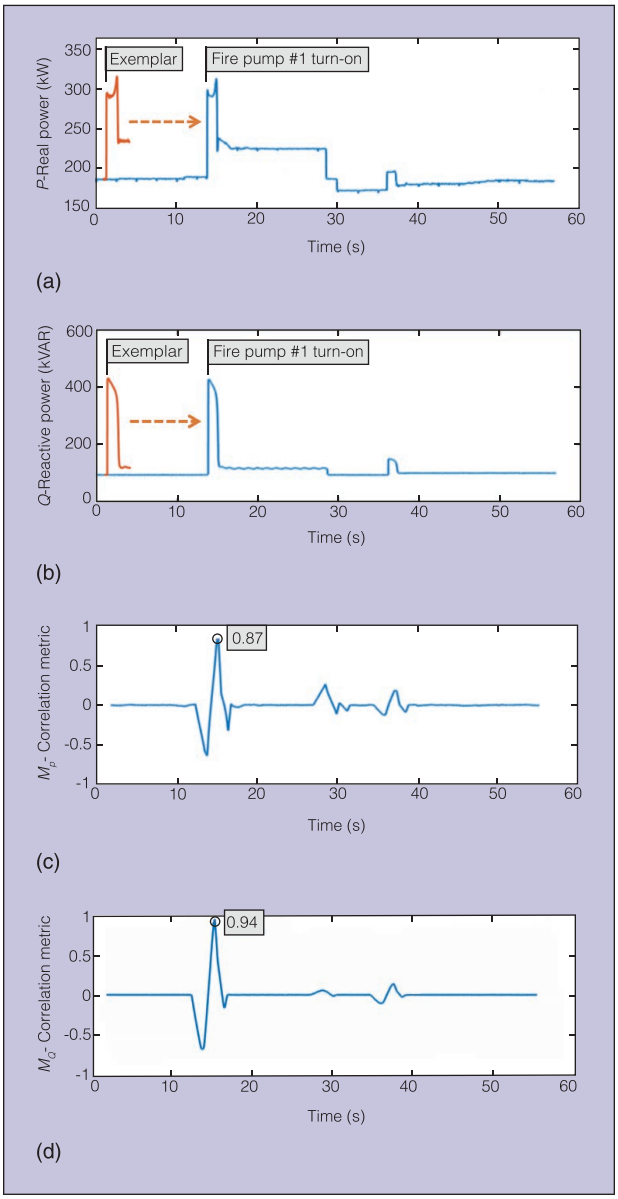

Fig. 7. Trainola performance using the first fire pump #1 transient as the exemplar around the time of the third fire pump #1 transient.

Creating a Database With Labeled Events

To date, this noncontact NILM system has collected data throughout multiple operational patrols, as well as several months with the ship stationed in port in Boston, MA. Data collected during each patrol are retrieved following the SPENCER's return to port. During this time, the sensors are checked to ensure they are still tightly attached to the cables, which they usually are. Thus, recalibration is not usually required. However, on rare occasions we found sections of improbable power data between two hours and several days in length (e.g., power flow *into* a generator). Typically, the NILM system recovers without intervention. Potential reasons for these periods of inconsistent data could be field interference from rarely energized equipment not accounted for during calibration or software bugs causing errors in the data processing. Efforts to better understand this issue are underway, including testing magnetic shielding as part of revisions to the sensors.

Fig. 8 shows an approximately nine-day period of aggregate real power data collected while the vessel was underway and returned to port. In this figure, the red, green, and blue traces indicate the three-phase power supplied by generator 1, generator 2, and fore shore power, respectively. While the ship is underway, from Dec. 24th through Dec. 30th, each generator alternates supplying power to the ship interspersed with periods of both generators supplying power. Early on Dec. 31st, the ship pulled into port, connected to shore power, and shut down the two diesel generators. In these traces, the darker solid line

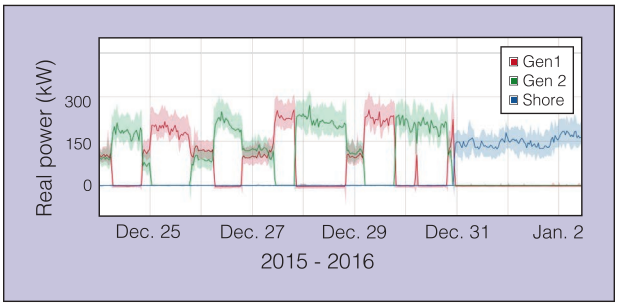

Fig. 8. Nine-day period of three-phase power measurements from the three power sources utilized: generator 1 (red), generator 2 (green), and fore shore power (blue).

signifies a decimated moving average of the recorded power, while the lighter shaded region gives an indication of the local variance of the power values about the mean trace.

Methods for disaggregating power streams typically fall into two categories, event-based or non-event based, which generally utilize supervised and unsupervised machine learning techniques, respectively [7]. For supervised techniques, algorithms require labeled data for training, while unsupervised techniques do not. Even so, labeled data aids in cross-validating the performance of unsupervised techniques. To begin compiling a dataset useful for both categories of load disaggregation, events are manually labeled by correlating electrical transients in the data streams to previously measured load "exemplar" waveforms around times when crew logs specifically recorded events, e.g., energizing a fire pump. These exemplar waveforms are short data streams captured in coordination with the crew, who energized and de-energized specified loads while we marked the transients in the data streams.

The loads with at least one identified exemplar are listed in Table 1. These loads are primarily pumps ranging in size from 3 kW to 56 kW. A watchstander records the operation of these loads, except for the gray water pumps, which operate automatically. These records provide an opportunity

Table 1 – Initial set of confirmed load exemplars from the first monitored operational patrol

Load Name	Electrical Specifications	Logged Operational Events			
		Labeled		Minimum Unlabeled	
		On	Off	On	Off
Watchstander Logged Loads					
Fire Pump 1	56 kW 0.88 PF	8	8	0	0
Fire Pump 2	56 kW 0.88 PF	3	3	0	0
Aft Steering Pump 1	22 kW 0.85 PF	6	6	0	0
Aft Steering Pump 2	22 kW 0.85 PF	6	6	0	0
CPP Pumps	7.5 kW 0.80 PF	11	8	9	10
Inport ASW Pump	7.5 kW 0.79 PF	2	2	1	1
Underway ASW Pump	11 kW 0.79 PF	2	2	1	1
Diesel Engine Auxiliary Loads					
Jacket Water Heater	9 kW 1 PF	13	13	34	34
Lube Oil Heater	12 kW 1 PF	13	13	34	34
Pre-Lube Pump	3 kW 0.8 PF	13	13	34	34
Other Loads					
Gray Water Pump	3.7 kW 0.79 PF	7	7	N/A	N/A

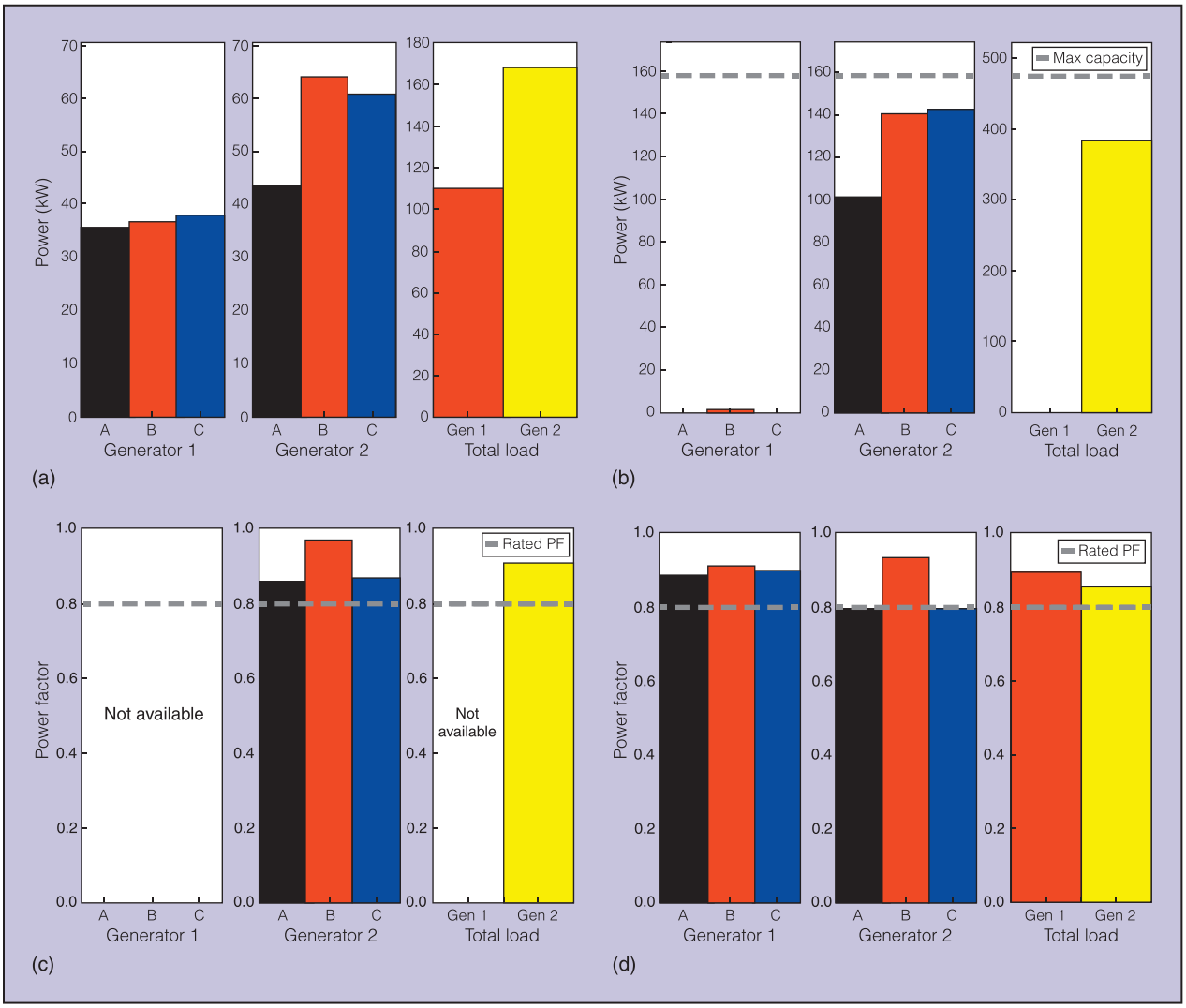

Fig. 9. Generator operation metrics showing load balancing between phases and each generator, and power factor for each phase and each generator. (a) Dec. 27, 2015, 1140:50 - Load Balance. (b) Dec. 28, 2015, 1342:32 - Load Balance. (c) Dec. 27, 2015, 1140:50 - Power Factors. (d) Dec. 28, 2015, 1342:32 - Power Factors.

to check the accuracy and precision of machine identification. The number of on and off events confirmed with a high level of confidence is shown in the "Labeled" (3rd and 4th) columns of the table. The 5th and 6th columns, entitled "Minimum Unlabeled," correspond to events indicated in the machinery logs, but whose corresponding electrical transients were not identified with a high level of confidence. This could be due to mislabeled or mistimed entries in the logs, or other simultaneous events, or both. Still, it remains likely that in many cases the recorded event occurred around the time logged. Thus, that an unlabeled transient occurred can still be useful information in developing disaggregation algorithms.

The gray water tanks are located in close proximity to the meters. As such, it was easy to note the timing of the tank pump run events during in port testing of the noncontact NILM system. Thus, several exemplar waveforms were identified for use with the Trainola correlation feature, however no estimate of the total number of events is available.

Automated Testing Applications

We used the dataset described above and the baseline transient detection algorithm, Trainola, to investigate several automated analysis applications: measuring and reporting power system metrics, generating watchstander log reports, and condition monitoring for cyclic loads.

Generator Operation Metrics

In addition to performing load-disaggregation based monitoring tasks, the noncontact NILM system also affords opportunities for generator monitoring. The processed power data streams are available in near real-time for metrics concerning the health of the generation and distribution system. These metrics can then be reported to crewmembers instigating further investigation if required.

Two mechanisms for load-induced failure in diesel generators such as those aboard the SPENCER are imbalanced loads and low power factor loads. Imbalanced current demands on the three phases of the generator can cause poor

Table 2 – Comparison of manually generated log to NILM detected events. In this table, MPDE is an acronym for Main Propulsion Diesel Engine, E/R stands for Engine Room, RMD stands for Restricted Maneuvering Doctorine, and CPP stands for Controllable Pitch Propeller.

Time	Event	Manual Log	NILM Log	Notes
1505	Secured both MPDE	✓	✓	NILM does not distinguish engines
1509	Energized #1 fire pump	✓	✓	NILM does not distinguish pumps
1515	Secured #1 fire pump	✓	✓	NILM does not distinguish pumps
1520	Secured both steering pumps	✓	✓	NILM does not distinguish pumps
1530	Round of E/R	✓		No exemplar transient for NILM
1540	Secured from Special Sea	✓		No exemplar transient for NILM
1540	Secured from RMD	✓	✓	Recorded at 1541 by NILM
1541	Secured both CPP "C" pumps		✓	Not recorded by watchstander
1602	Swapped potable water suction	✓		No exemplar transient for NILM
1655	Singled electrical load on Gen. #2		✓	Watchstander log indicates incorrect Gen.
1707	Secured Gen. #1	✓	✓	Recorded at 1653 by NILM
1843	Started both MPDE		✓	Not recorded by watchstander
1900	Secured both MPDE	✓	✓	NILM does not distinguish engines
1903	Commenced fuel transfer	✓	✓	Recorded at 1912 by NILM

efficiencies, thermal and mechanical stresses [8], [9], and vibrations that increase the noise signature of the ship [10]. Low power factor loads require increased currents for a given power demand. Thus, low power factors limit the generator capability.

The NILM system can generate metrics of phase balance and power factor and report them to the crew in near real-time. Fig. 9 shows an example of such metrics. The figure features bar plots reporting each generator's loading by phase as well as a comparison of overall loading between generators on Dec. 27, 2015 at 1140:50 (Fig. 9a) and Dec. 28th at 1342:32 (Fig. 9b). From Fig. 9a, crew operators can immediately note that while Generator 1 is well balanced, Generator 2 is not. Instead, Phase B is roughly 40% more loaded than Phase A, and Generator 2 is about 50% more loaded overall than Generator 1. At 1342:32 on Dec. 28th, the plot shows that now only generator 2 is operating, and while it is slightly more balanced, the generator is nearing its maximum capacity.

Operating at this capacity, however, requires an operating power factor of at least 0.8. The power factors for each generator are similarly reported in Fig. 9c and Fig. 9d. Fig. 9c shows that each phase of both generators are operating near or above their rated power factor levels on Dec. 27th at 1140:15. Similarly, Generator 2 is operating above the rated power factor level on Dec. 28th at 1342:32 (Fig. 9d). Thus, the real power demanded of the generator at this time is still in compliance with the generator's power delivery capabilities.

Automated Machinery Log

The machinery log is an official document, and in the event of an accident caused by machinery malfunction or operator error, the document becomes a legal reference in court. Thus, it is important that these logs be accurate. Further, automating log generation helps to modernize the marine environment by reducing crew time commitments dedicated to low-level manual tasks. The noncontact NILM system can aid in both objectives. Specifically, given a crew-generated log with rough timings of events, it can identify exact times of transients corresponding to the log events, thus improving the log accuracy. Ultimately, as improved event detection and identification algorithms are applied, the need for a crew-generated log disappears entirely.

The NILM's ability to automatically log events is contrasted against the manual log for a four-hour period on Dec. 24th, 2015 (Table 2). Each event recorded by the watchstander is listed with the time in the first column and a shortened description in the second. Typically recorded events, which were identified by the NILM but *not* recorded by the watchstander, are also shown, e.g., 1541 - "Secured both CPP "C" pumps." Check marks indicate if the event was recorded in the manually generated log and the NILM generated log, respectively.

Of the twelve events listed by the officer, the NILM system is able to automatically record nine. Currently, the NILM system cannot distinguish well between identical loads, e.g., fire pumps #1 and #2, as their transients are extremely similar and thus well correlated. Some events, such as "round of E/R," which means the watchstander inspected the equipment in the engine room, provide no electrical transient for the NILM system to detect. The NILM system did indicate that the watchstander missed recording events typically included in the log and incorrectly recorded other events. Notably, at 1655 the watchstander recorded that all electrical loads were singled on Generator #1, though the data streams at that time show Generator #2 singling the loads. Regarding the events detected by

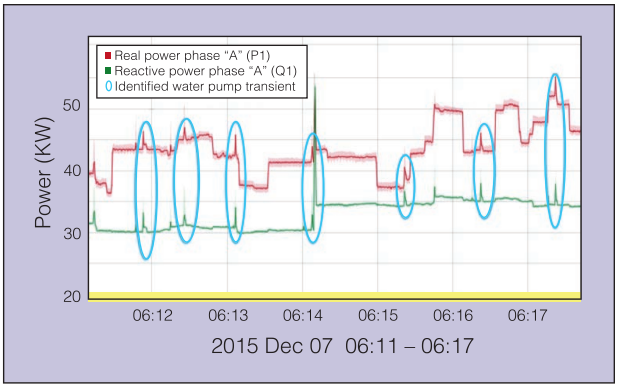

Fig. 10. Real and reactive power streams showing the detected short cycling gray water pump.

the NILM but not recorded by the watchstander, it is certainly possible that these events are false positive detections. However, at least in the case of the "Secured both CPP "C" pumps" event at 1541, being secured from RMD almost always corresponds to also securing the CPP "C" pumps, thus giving a high level of confidence that the event did indeed occur.

Cyclic Load Condition Monitoring

A final application for the noncontact NILM system is condition monitoring. By detecting and assigning transients to specific loads or simply grouping together transients with similar traits, the NILM system can detect changes in event timing patterns, which can be indicative of machinery faults [11]. This is particularly important in closed-loop controlled loads, e.g., cyclic loads such as gray water tank pumps, as precatastrophic faults can easily go unnoticed.

The gray water waste system aboard the SPENCER collects the wastewater from non-sewage and non-recycling water loads such as sinks, showers, and washers. This waste is collected in a holding tank before being filtered and pumped overboard or combined with sewage, depending on the ship's location and local pollution regulations. Tank level indicators (TLIs) provide feedback to the pump's control system, indicating when the water level is high and needs to be pumped down.

Using exemplar waveforms of such pump runs, the Trainola function reported very high-frequency pump operation but with very short run times. Fig. 10 depicts this short cycling operation. The phase A real and reactive power streams are plotted over a seven minute period on Dec. 7, 2015. During this period, seven transients indicative of pump runs were identified by the NILM system, but these transients only lasted a few seconds.

A common failure mode for the gray water pumps occurs when the is TLI sensors become clogged with debris and oil, leading to premature "full tank" indications and causing the pumps to shut off only a few seconds after switching on. Eventually this leads to pump failure by overworking the pump and working it with no discharge fluid. On the SPENCER, this fault was the root cause of the pump's short cycle operation. However, the fault had gone unnoticed by the crew as the control system still moves gray water on from the tank and full failure had not yet happened. Thus, the NILM system can detect such faults before they cause failure and can be automated to do so by monitoring the statistical distributions of the pump's run frequency and run length [12].

Conclusion

Noncontact current and voltage sensors represent next-generation sensor technology for NILM systems. As shown through their application aboard the U.S. Coast Guard SPENCER, these sensors, when combined with signal processing and signal disaggregation techniques, create a powerful tool for automated testing of electrical systems and loads. These sensors are easy to install and uninstall, making them useful for crew technicians needing to perform on-the-go diagnostic tests of subsystems or individual pieces of equipment.

The data collected from the USCGC SPENCER have been matched against manually generated machinery logs in order to build a dataset for testing disaggregation algorithms. With the sensors still installed aboard the ship, more data are continuously being collected and new instances of machinery events identified. Moving forward, we plan to develop and apply more advanced disaggregation, condition monitoring, and energy scorekeeping algorithms to further improve the autonomy, accuracy, and automated testing abilities of the noncontact system.

Acknowledgment

The authors thank the crew of the U.S. Coast Guard Cutter SPENCER for their service as well as their generosity and technical support in accessing and understanding ship systems and operations.

References

[1] J. S. Donnal and S. B. Leeb, "Noncontact power meter," *IEEE Sensors J.*, vol. 15, no. 2, pp. 1161–1169, Feb. 2015.

[2] C. Laughman, K. Lee, R. Cox, S. Shaw, S. Leeb, L. Norford, and P. Armstrong, "Power signature analysis," *IEEE Power and Energy Mag.*, vol. 1, no. 2, pp. 56–63, Mar. 2003.

[3] United States Coast Guard, U.S. Dept. of Homeland Security, Mar. 2017. [Online]. Available: www.uscg.mil.

[4] A. Zoha, A. Gluhak, M. A. Imran, and S. Rajasegarar, "Non-intrusive load monitoring approaches for disaggregated energy sensing: a survey," *Sensors*, vol. 12, no. 12, pp. 16 838–16 866, 2012.

[5] J. Paris, J. S. Donnal, and S. B. Leeb, "Nilmdb: the non-intrusive load monitor database," *IEEE Trans. on Smart Grid*, vol. 5, no. 5, pp. 2459–2467, Sep. 2014.

[6] J. Donnal, J. Paris, and S. B. Leeb, "Energy applications for an energy box," *IEEE Internet of Things J.*, vol. PP, no. 99, pp. 1–1, 2016.

[7] J. Paris, J. S. Donnal, Z. Remscrim, S. B. Leeb, and S. R. Shaw, "The spectral envelope preprocessor," *IEEE Sensors J.*, vol. 14, no. 12, pp. 4385–4394, Dec. 2014.

[8] T. F. Chan and L. L. Lai, "Steady-state analysis and performance of a stand-alone three-phase induction generator with asymmetrically connected load impedances and excitation capacitances," *IEEE Trans. Energy Conversion*, vol. 16, no. 4, pp. 327–333, Dec. 2001.

[9] E. Muljadi, R. Schiferl, and T. A. Lipo, "Induction machine phase balancing by unsymmetrical thyristor voltage control," *IEEE Trans. Industry Applications*, vol. IA-21, no. 3, pp. 669–678, May 1985.

[10] R. Zachar, P. Lindahl, J. Donnal, W. Cotta, C. Schantz, and S. B. Leeb, "Utilizing spin-down transients for vibration-based diagnostics of resiliently mounted machines," *IEEE Trans. Instrum. Meas.*, vol. 65, no. 7, pp. 1641–1650, Jul. 2016.

[11] J. Paris, J. S. Donnal, R. Cox, and S. Leeb, "Hunting cyclic energy wasters," *IEEE Trans. on Smart Grid*, vol. 5, no. 6, pp. 2777–2786, Nov. 2014.

[12] J. C. Nation et al., "Nonintrusive monitoring for shipboard fault detection,in *Proc. 2017 IEEE Sensors Applications Symposium (SAS)*, pp. 1–5, 2017.

[13] P. Lindahl, S. Leeb, J. Donnal, and G. Bredariol, "Noncontact sensors and nonintrusive load monitoring (NILM) aboard the USCGC spencer," in *Proc. IEEE AUTOTESTCON 2016*, pp. 1-10, DOI: 10.1109/AUTEST.2016.7589633.

Peter Lindahl is a Postdoctoral Associate working in the Laboratory for Electromagnetic and Electronic Systems, a subsidiary of the Research Laboratory of Electronics at the Massachusetts Institute of Technology (MIT). He graduated with his Ph.D. degree in engineering from Montana State University in 2013 after receiving his B.S. degree in electrical engineering from Pennsylvania State University in 2003. Dr. Lindahl's research focuses on advanced energy applications from smart-meters to micro-grids, with particular interests in sensors and instrumentation development, signal processing, system identification and modeling, and system control.

Greg Bredariol is a U.S. Coast Guard officer and a mechanical engineering M.S. degree candidate at MIT. Lt. Bredariol graduated from the U.S. Coast Guard Academy in 2015. Working under the direction of Dr. Steven Leeb in the Research Laboratory of Electronics at MIT, he has directed applications of novel sensors and instrumentation in military environments including USCGC ships and US Army bases.

John Donnal is an Assistant Professor at the U.S. Naval Academy in the Weapons and Systems Engineering Department. A former U.S. Army Officer, John received his B.S. degree in electrical engineering from Princeton University in 2007 and his M.S. and Ph.D. degrees in electrical engineering from MIT in 2013 and 2016, respectively. Dr. Donnal's research interests include cyber-physical systems, nonintrusive load monitoring synthesis, energy harvesting, and communication systems.

Steven B. Leeb received the Ph.D. degree from MIT in 1993 and has been a Faculty Member with the Department of Electrical Engineering and Computer Science at MIT since 1993. He also holds a joint appointment with the Department of Mechanical Engineering, MIT. Dr Leeb's research is concerned with the development of signal processing algorithms for energy and real-time control applications.